VARIABLE SAMPLE ILLUMINATION AND ANGULAR MAGNIFICATION FOR THE RUEDI ULTRAFAST ELECTRON DIFFRACTION BEAMLINE

S. S. Percival*, A. R. Bainbridge, B. R. Hounsell, J. W. McKenzie
ASTeC and Cockcroft Institute, STFC Daresbury Laboratory, Warrington, UK

Abstract

The RUEDI (Relativistic Ultrafast Electron Diffraction & Imaging) ultrafast electron diffraction (UED) beamline aims to deliver MeV electron bunches for sub-10 fs timescale diffraction experiments. The achievable momentum transfer resolution of the diffraction pattern at the detector is determined by the quality and focusing of the beam at the sample, and the transport of the diffracted beam to the detector. A beamline design is presented which allows for flexible illumination onto the sample and variable angular magnification. The pre-sample electron optics consist of two apertures and two single-solenoid lenses followed by the post-sample optics which consist of two double-solenoid lenses. Simulated results are used to demonstrate the range of capabilities of each system and show that RUEDI will be capable of producing the high-resolution diffraction patterns needed for a world-leading UED machine.

INTRODUCTION

RUEDI is a proposed user facility composed of two beamlines, a single-shot, time-resolved MeV imaging line, and an ultrafast MeV diffraction line with sub-10 fs temporal resolution [1, 2]. The diffraction line will consist of an S-band RF photoinjector [3], a magnetic compression arc and variable electron optics with a large variety of sample pumps and environments available. The design of the electron optics, consisting of a pre-sample condenser system for variable sample illumination and a post-sample projection system for angular magnification onto the detector, are outlined here.

VARIABLE ILLUMINATION

The pre-sample condenser optics allow for the tuning of the bunch charge, spot size and angular convergence onto the sample for different experiments. The condenser section of the beamline, as shown in Fig. 1, consists of two apertures alternating with two single-solenoid lenses. The beam entering the condenser section of the machine is the same for all modes: a 4 MeV, 400 fC bunch undergoing ballistic compression from the magnetic arc which leads to a temporal focus at the sample. This method of temporal compression requires there to be a large energy chirp across the beam, which increases the impact of chromatic aberration effects throughout the beam transport. The two apertures are used to cut the charge of the bunch to a variety of charges from 1.6 fC for stroboscopic experiments up to 160 fC for single-shot experiments.

* suzanna.percival@stfc.ac.uk

The different illumination modes provide a trade-off between coherence length, spot size, and the number of electrons hitting the sample. The quality of the bunch at the sample is quantified by its coherence length, L_c, which determines the minimum achievable momentum transfer (Q) resolution, ΔQ_{RMS}, at the detector. The relationship between these two values and their definition with respect to the electron beam properties at the sample are given by

$$\Delta Q_{\mathrm{RMS}} \approx \frac{1}{L_c} = \frac{2\pi\varepsilon_x}{\lambda\sigma_x} = \frac{2\pi\sigma_{x'}}{\lambda}, \qquad (1)$$

where ε_x is the geometric transverse emittance, λ is the de Broglie wavelength of the electrons, σ_x is the RMS beam size, and $\sigma_{x'}$ is the RMS uncorrelated divergence of the beam. This assumes that the sample size and energy spread contributions to ΔQ_{RMS} are negligible. Other key parameters include the bunch length which can be affected by strong space charge forces at transverse focuses, and the transverse size of the beam.

The main illumination mode used in diffraction experiments is with the beam focused parallel onto the sample. This improves the Q resolution as the larger beam at the sample reduces the uncorrelated beam divergence and so reduces the contribution of this divergence to the angle of the diffracted beam. This mode gives the best pattern quality and temporal resolution of any mode, but has a limited smallest spot size [4]. Other modes of interest include: a converging illumination mode, which focuses the bunch so it converges onto the sample allowing for higher charge density with minimal focusing, but as this does not have parallel illumination, projector optics are required to focus the resulting diffraction pattern onto the detector; and a small-spot mode which strongly focuses the bunch creating a crossover, allowing for micro-diffraction experiments [5], but with worse temporal resolution due to space charge forces, and detrimental effects on the pattern quality.

Figure 2 shows a comparison of how the beam will be cut and focused by the apertures and solenoids for these three illumination modes. For the parallel and converging modes, the first solenoid lens is used to focus the beam parallel onto the second aperture which cuts the charge. The second solenoid is then used to choose the focus of the beam onto the sample. Cutting the charge in the second aperture removes the outer particles of the bunch as late as possible and so reduces space charge driven emittance growth.

For the small-spot mode, the charge is cut in the first aperture to decouple the charge delivered to the sample from the tuning of the first solenoid. The first solenoid is then used to focus the beam into a transverse crossover such that the beam size at the second solenoid is larger than at the first. The

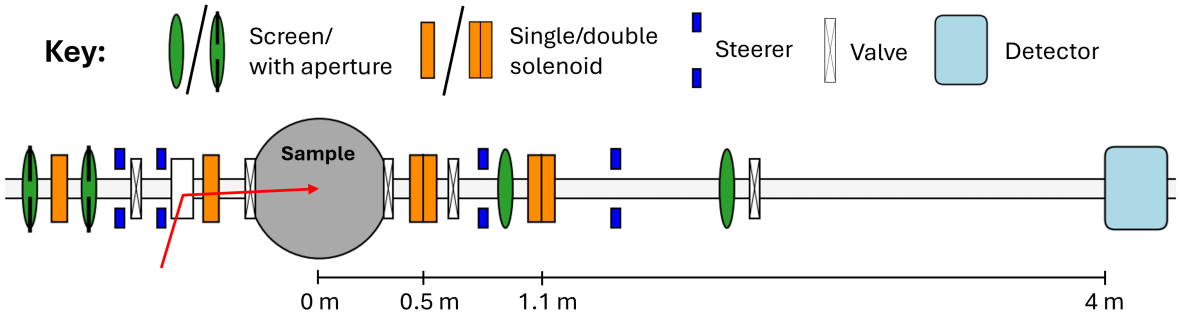

Figure 1: Schematic showing the condenser and projector sections of the RUEDI diffraction line.

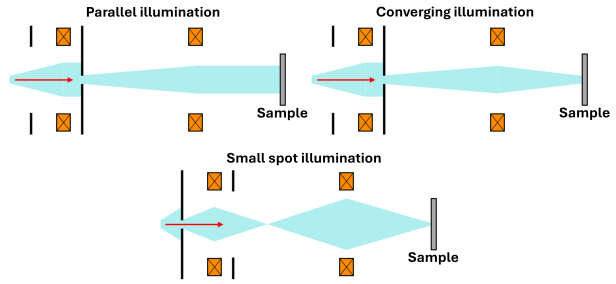

Figure 2: Diagrams of how the condenser apertures and solenoids are used for different sample illumination modes. The red arrow indicates the direction of electron travel.

second solenoid then sharply focuses the beam into a waist on the sample, which approximates parallel illumination as the beam divergence at a waist is uncorrelated.

Simulations were carried out using General Particle Tracer (GPT) [6] to determine the achievable beam parameters at the sample. The results for the parallel and small-spot modes can be seen in Table 1. For the small-spot mode, beam sizes as low as 32 µm FW diameter can be achieved for a 1.6 fC bunch while keeping the bunch length to 18.6 fs and the transverse emittance increase in comparison to the parallel mode to only 11%. However, the increase in bunch length and transverse emittance for the larger 160 fC charge are much more prevalent in the small-spot mode.

Table 1: Beam Parameters at the Sample

	Parallel		**Small-spot**	
Charge [fC]	1.6	160	1.6	160
FWHM t [fs]	5.7	9.2	18.6	95.7
FW diameter [µm]	168	1670	32	417
$\varepsilon_{n,x}$ [nm rad]	2.02	26.8	2.22	41.5
$\varepsilon_{n,y}$ [nm rad]	1.96	29.4	2.17	38.2
B_{4D} [fC/nm rad^2]	0.41	0.20	0.33	0.10
L_C [nm]	7.0	5.8	0.93	0.83
ΔQ_{RMS} [Å^{-1}]	0.014	0.017	0.11	0.12

Solenoid strength limitations are an issue for the small-spot mode where the second solenoid needs to focus the very large and diverging beam sharply to form a waist at the sample downstream. In simulation, this required peak field strengths of up to 370 mT, so a pole-piece enhanced solenoid with a short, strong field should be used.

ANGULAR MAGNIFICATION

The post-sample projector optics allow for variable angular magnification of the scattered electrons onto the detector. Following the sample chamber, the bunch passes through a two solenoid imaging system, as seen in Fig. 1, similar to that used at Osaka [7,8], and at the SLAC MeV UED facility which used permanent magnet solenoids [9]. A two lens system was chosen for its variable magnification capabilities, which remove the limitations placed on measured Q resolution by the size of the detector and its pixelation. Instead, the resolution is only limited by the coherence length of the bunch at the sample, as defined in Eq. (1), and the transport of the scattered bunch.

The first lens (the diffraction lens) focuses the beam onto its back focal plane and converts the scattering angle of the diffracted beam into transverse position. The second lens (the projection lens) then magnifies this image onto the detector, for a total of $\frac{3}{2}\pi$ phase advance. This system can be described using the transfer matrices,

$$\begin{pmatrix} x_f \\ x_f' \end{pmatrix} = \begin{pmatrix} m & 0 \\ m' & \frac{1}{m} \end{pmatrix} \begin{pmatrix} 1 & f_0 \\ 0 & 1 \end{pmatrix} \begin{pmatrix} 1 & 0 \\ -\frac{1}{f_0} & 1 \end{pmatrix} \begin{pmatrix} x_i \\ x_i' \end{pmatrix} \quad (2)$$

where x_i and x_i' are the particle's spatial and momentum coordinates at the sample, x_f and x_f' the coordinates at the detector, f_0 is the focal length of the diffraction lens, m is the magnification and m' is the axial derivative of m at the detector [10, 11]. The magnification is determined by the camera length of the projection system. For a drift, this is the distance from the sample to the detector, L_0. For a two lens system the (effective) camera length is given by

$$C_L = \frac{L_2 L_4}{L_3} = mL_0 \quad (3)$$

where L_2, L_3 and L_4 are the distances as shown in Fig. 3. A larger camera length range therefore means a larger range of magnifications.

The two solenoid lenses are positioned at 0.5 m and 1.1 m, and the main detector at 4 m from the sample. The position of the projector lens is a trade-off between camera length range and Q resolution. Being further from the diffraction lens, up to an optimal distance of 2.3 m from the sample, increases the range of camera lengths that can be achieved, after which the range decreases again. Being as close as

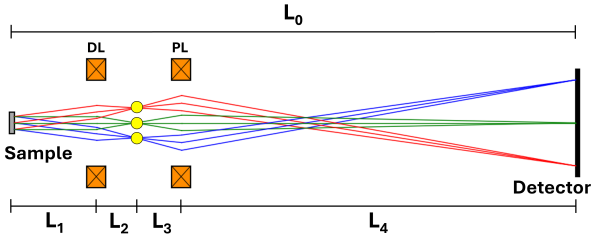

Figure 3: Ray diagram of projector system. The yellow dots indicate the back focal plane of the diffraction lens (DL), and the three different ray colours represent three different initial particle angles.

possible to the diffraction lens improves the Q resolution as there is less distance over which the beam can expand so the beam stays small in the solenoids, minimising the chromatic aberration effects that result from the large energy spread across the bunch required for compression. Similarly, moving the detector further from the sample allows for longer camera lengths, but increases the footprint of the machine.

The length and strength of the lenses also affects the camera length range. Double-solenoids [12] were chosen to minimise the effects of Larmor rotation on the scattered beam, but this makes the field longer and weaker. A longer field limits the camera length as, for the maximum camera lengths where the strength of the diffraction lens is such that its back focal plane is within its own field, the bunch undergoes more focusing after passing through its waist. This causes the camera length to deviate from the thin-lens approximation assumed in Eq. (3). To counteract this, an improved double-solenoid with a shorter, stronger field profile was designed by adding shaped pole pieces to the yoke, achieving a camera length much closer to the thin-lens approximation.

Simulations of a diffracted 16 fC parallel illumination beam transported through the projector system were used to determine the achievable camera lengths and Q resolutions for different lens designs and arrangements. The scattering of the beam was calculated using a GPT custom element. The strength of the two lenses were varied in opposition to scan the position of the back focal plane and so the camera length as seen in Eq. (3), whilst maintaining the imaging condition. To calculate the Q resolution, the diffraction pattern at the detector is histogrammed according to momentum transfer, then the Q resolution, ΔQ_{FWHM}, is calculated as the average FWHM of the peaks. The results of these simulations are shown in Fig. 4, comparing a single-solenoid with a maximum field strength of 268 mT to the improved double-solenoid with a maximum strength of 421 mT. The projection lens is compared at two distances from the sample. The 'at sample limit' is defined as in Eq. (1), then converted from RMS to FWHM approximating the peaks as Gaussian.

The Q resolutions shown in Fig. 4 are largely unaffected by the choice of lens design. Instead, the sharp increase in Q resolution seen at lower camera lengths is due to the aberration effects of the projector lens. Smaller camera lengths are achieved by using a stronger diffraction lens to move the back focal plane upstream, leading to a larger bunch

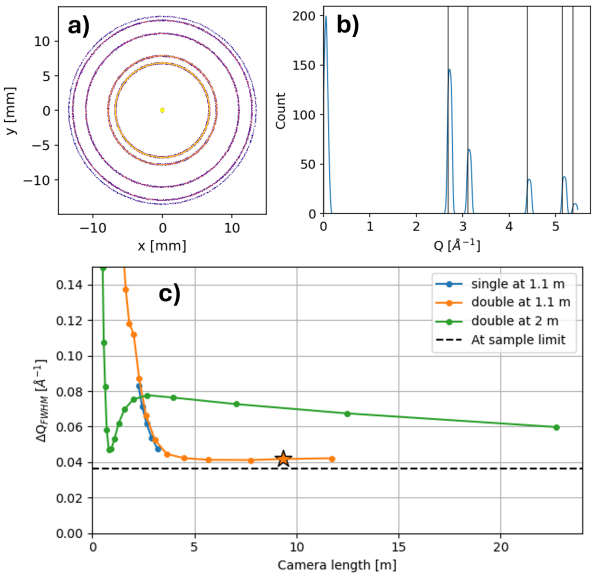

Figure 4: Simulated results of using projectors to transport the diffracted beam. a) An example of the diffraction pattern at the detector. b) The diffraction pattern histogrammed according to momentum transfer. c) Q resolution for the full camera length range of the single vs double solenoid, and with the projection lens positioned 1.1 m or 2 m from the sample. The star indicates the point shown in a) and b). The at sample limit is as defined by Eq. (1).

in the projector lens and so increasing aberration based Q resolution degradation. In the case where the projector lens is positioned 2 m from the sample, good Q resolutions can only be achieved for a very small camera length range, all of which is under 4 m resulting in demagnification, as these are the only camera lengths where the bunch is small in the projection lens. The camera length range that has a Q resolution below 0.05 Å^{-1}, using the optimised double-solenoid with the projector lens at 1.1 m from the sample, is 3.25 m to 11.73 m, equivalent to 0.8 x to 2.9 x magnification.

CONCLUSION

A design is presented for the RUEDI ultrafast electron diffraction line electron optics. A pair of condenser lenses and apertures are used to tune for different illumination modes, achieving up to 0.41 fC/nm rad^2 brightness with sub-10 fs bunch length at the sample. Two lenses are then used to image and magnify the scattered beam, achieving sub-0.05 Å^{-1} Q resolution for camera lengths 3.25 m to 11.73 m. Future design work will focus on further improving the magnet design to widen the capabilities of both systems.

ACKNOWLEDGEMENTS

We would like to thank the contributions from the wider RUEDI team, especially Yoshie Murooka for insight into UED optics. We would also like to thank Lydia Hall for the development of the diffraction GPT custom element.

REFERENCES

[1] J. W. McKenzie *et al.*, "Status of the RUEDI UK national facility design", in *Proc. IPAC'24*, Nashville, TN, USA, pp. 1979–1982, May 2024. doi:10.18429/JACoW-IPAC2024-WEPC13

[2] B. R. Hounsell *et al.*, "An update of progress on the design of the diffraction line for the relativistic ultrafast electron diffraction and imaging facility at Daresbury Laboratory", in *Proc. IPAC'25*, Taipei, Taiwan, Jun. 2025, pp. 1208–1211. doi:10.18429/JACoW-IPAC2025-TUPM021

[3] L. S. Cowie *et al.*, "RF design of the 1 kHz photoinjector for the RUEDI electron diffraction facility", presented at IPAC'26, Deauville, France, May 2026, paper TUP3074, this conference.

[4] D. Filippetto *et al.*, "Ultrafast electron diffraction: Visualizing dynamic states of matter", *Rev. Mod. Phys.*, vol. 94, no. 4, p. 045004, Dec. 2022. doi:10.1103/RevModPhys.94.045004

[5] X. Shen *et al.*, "Femtosecond mega-electron-volt electron microdiffraction", *Ultramicroscopy*, vol. 184, pp. 172–176, 2018. doi:10.1016/j.ultramic.2017.08.019

[6] M. J. de Loos and S. B. van der Geer, "General Particle Tracer: A New 3D Code for Accelerator and Beamline Design", in *Proc. EPAC'96*, Sitges, Spain, Jun. 1996, paper THP001G, pp. 1241–1243.

[7] Y. Murooka, N. Naruse, S. Sakakihara, M. Ishimaru, J. Yang, and K. Tanimura, "Transmission-electron diffraction by MeV electron pulses", *Appl. Phys. Lett.*, vol. 98, no. 25, p. 251903, Jun. 2011. doi:10.1063/1.3602314

[8] J. Yang, K. Gen, N. Naruse, S. Sakakihara, and Y. Yoshida, "A compact ultrafast electron diffractometer with relativistic femtosecond electron pulses", *Quantum Beam Sci.*, vol. 4, no. 1, p. 4, 2020. doi:10.3390/qubs4010004

[9] C. J. R. Duncan *et al.*, "Enhancing reciprocal space resolution in mev ultrafast electron diffraction with permanent magnet lenses", in *Proc. NAPAC'25*, Sacramento, CA, USA, Aug. 2025, pp. 439–441. doi:10.18429/JACoW-NAPAC2025-TUP037

[10] P. Denham *et al.*, "High energy electron diffraction instrument with tunable camera length", *Struct. Dyn.*, vol. 11, no. 2, p. 024302, Mar. 2024. doi:10.1063/4.0000240

[11] M. Reiser, P. O'Shea, S. Bernal, and R. Kishek, *Theory and design of charged particle beams*. Hoboken, NJ, USA: Wiley, Mar. 2008. doi:10.1002/9783527622047

[12] S. M. Juma and T. Mulvey, "Miniature rotation-free magnetic electron lenses for the electron microscope", *J. Phys. E: Sci. Instum.*, vol. 11, no. 8, p. 759, Aug. 1978. doi:10.1088/0022-3735/11/8/014